Supporting Information for

Axial forces in capillary liquid bridges of polymer solutions

Sreeram Rajesh[1], Riley S. Tinianov[1], Jooyeon Park[2], and Alban Sauret[2,3]

[1] *Department of Mechanical Engineering, University of California, Santa Barbara, California 93106, USA*
[2] *Department of Mechanical Engineering, University of Maryland, College Park, Maryland 20742, USA*
[3] *Department of Chemical and Biomolecular Engineering, University of Maryland, College Park, Maryland 20742, USA*

S1 Validating the experimental setup with silicone oil

To validate our force sensor setup, we measure axial force in a capillary liquid bridge formed by AP100 silicone oil (by Sigma-Aldrich). AP100 has very low viscosity ($\eta \simeq 100$ mPa.s) and surface tension ($\gamma = 24$ mN/m, as provided by the supplier), which also results in a small contact angle ($\theta = 0°$). For the validation test, the volume of silicone oil is also kept low to avoid any perturbation from gravity. We measure the volume $V = 0.036$ μL from the image analysis. The particles are separated quasi-statically. We show the capillary force F measured as the gap S increases in Fig. S1. The measured force is compared with the approximation derived from the Gorge method by Pitois *et al.* [1]:

$$F_{\text{Cap}} \approx 2\pi R\gamma\cos\theta\left[1-\frac{1}{\sqrt{1+\frac{2V}{\pi RS^2}}}\right] \tag{S1}$$

The experimental measurements agree well with this approximate equation, which is only valid for liquids with small contact angle ($\theta \simeq 0-10°$). Notably, for $V = 0.036$ μL, the experimental measurements follow the expected curve very closely. Furthermore, the measured rupture distance $S_{\text{rup}} = 0.345$ mm is close to the value estimated from the expression provided by Lian *et al.* [2] $(1+0.5\theta)V^{1/3} \simeq 0.33$ mm.

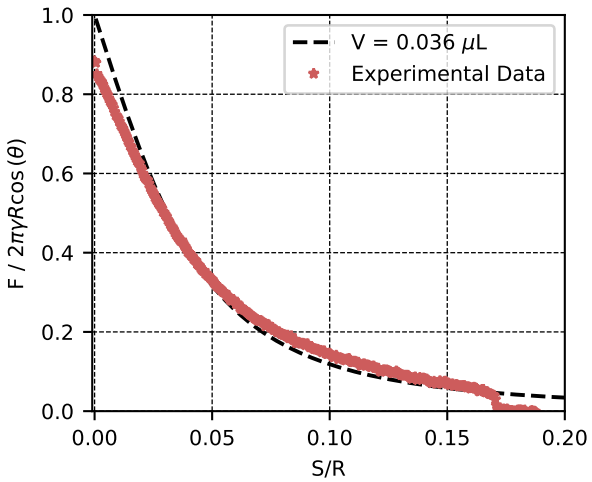

Figure S1: Axial force due to AP100 silicone oil of $V = 0.036$ μL on spherical particles measured using the force sensor based setup described in the main article.

S2 Shear Rheology: Viscosity and Modulus for 4M PEO solutions

We measured the shear viscosity (η), storage modulus (G'), and loss modulus (G'') of 4M PEO solutions (M_w = 4000 kg/mol) dissolved in water using a rheometer (Anton Paar MCR 302) with a 50 mm, 1° cone-plate geometry. The viscosity increases with concentration, and clear shear-thinning is observed for the polymer solutions shown in Fig. S2(a). The corresponding storage and loss moduli are reported in Fig. S2(b).

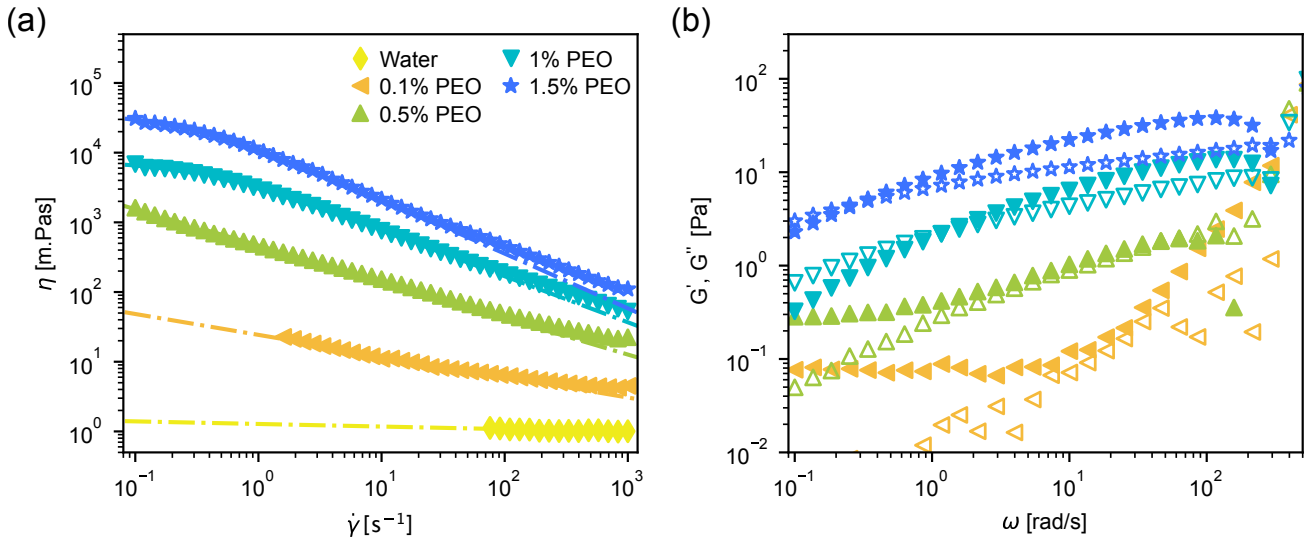

Figure S2: (a) Evolution of the shear viscosity η with shear rate $\dot{\gamma}$. (b) Storage modulus G' (solid symbols) and loss modulus G'' (open symbols) as functions of angular frequency ω for water and 4M PEO solutions at different concentrations.

S3 Extensional Rheology: Relaxation Time for 4M PEO solutions using Pendant Drop Method

To measure the relaxation time, we quantify the evolution of the minimum thickness of the neck in a droplet pinch-off, $h_{\min}(t)$. As noted in numerous previous studies [3, 4], the droplet pinch-off in the viscoelastic regime follows an exponential thinning characterized as: $h_{\min}(t) \propto e^{-t/3\lambda_R}$. By fitting the thinning dynamics in the exponential regime, we extract the relaxation time (λ_R) for the polymer solutions, summarized in Fig. S3. As noted in previous works, the relaxation time scales with the concentration of the polymer solution as

$$\lambda_R \propto c^{0.7} \tag{S2}$$

where the exponent of 0.7 is similar to values previously reported by Tirtaatmadja *et al.* [4] and Rajesh *et al.* [3].

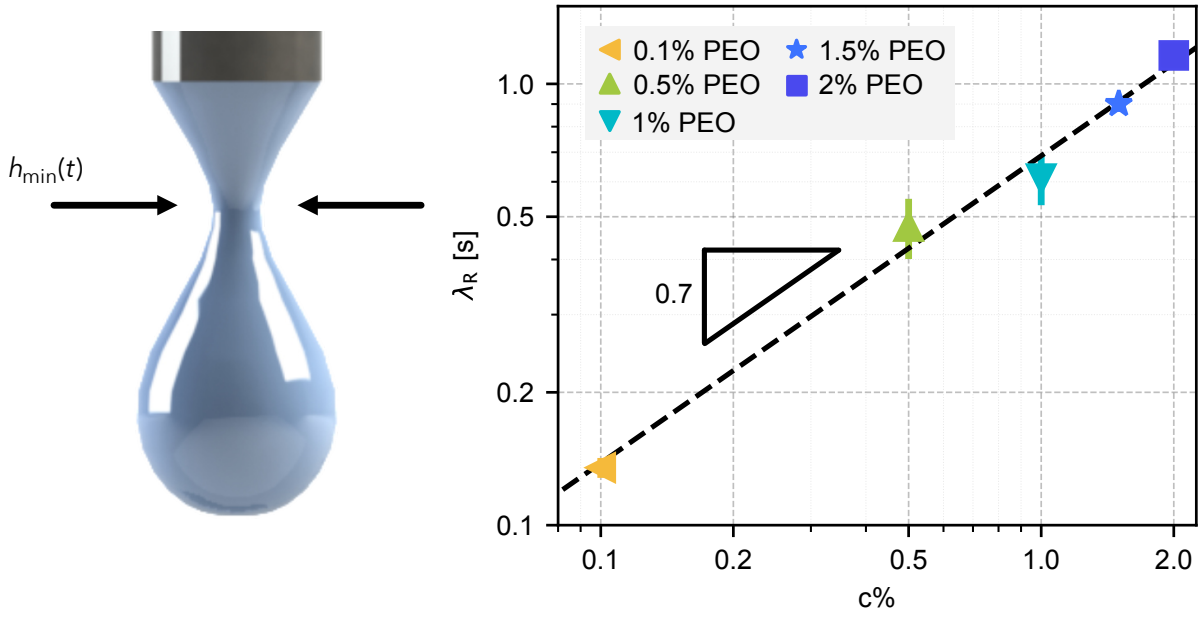

Figure S3: (a) Schematic of a droplet indicating how the minimum thickness of the thinning droplet is measured (b) Relaxation time of a 4M PEO solution at $c = 0.1 - 2$ % in water. The nozzle diameter used is $h_0 = 2.75$ mm.

S4 Surface Tension and Dynamic Solid-Liquid Contact Angle

In Fig. S4(a), we show the surface tension γ for the 4M PEO polymer solutions of various concentrations c prepared in water. As c increases, γ indeed decreases. For $c = 0.1$ – 1%, we are able to systematically quantify this using a tensiometer (Attension Theta Lite). For $c = 1.5\%$, the tensiometer measurements are inconsistent. However, from γ measurements for higher concentrations of high M_w polymer solutions, similar to the $M_w = 4000$kg/mol used in this study, noted in a previous work by Cao *et al.* [5], we do not expect γ to drop significantly for the $c = 1.5\%$ 4M PEO solution. Hence, we consider $\gamma = 60$ mN/m for the present work.

To quantify the solid-liquid contact angle θ (see Fig. 1(c) in the main article), we developed a custom image-analysis protocol to measure θ as a function of the separation gap S. In Fig. S4(b), we show $\theta(S)$ under quasi-static conditions ($v = 0.01$ mm/s). As shown here, θ decreases slightly with increasing c, which is expected due to the decrease in γ. This trend is slightly off for $c = 1\%$, but as noted in the main article, this deviation is attributed to the slightly lower volume of liquid dispensed in the liquid bridge.

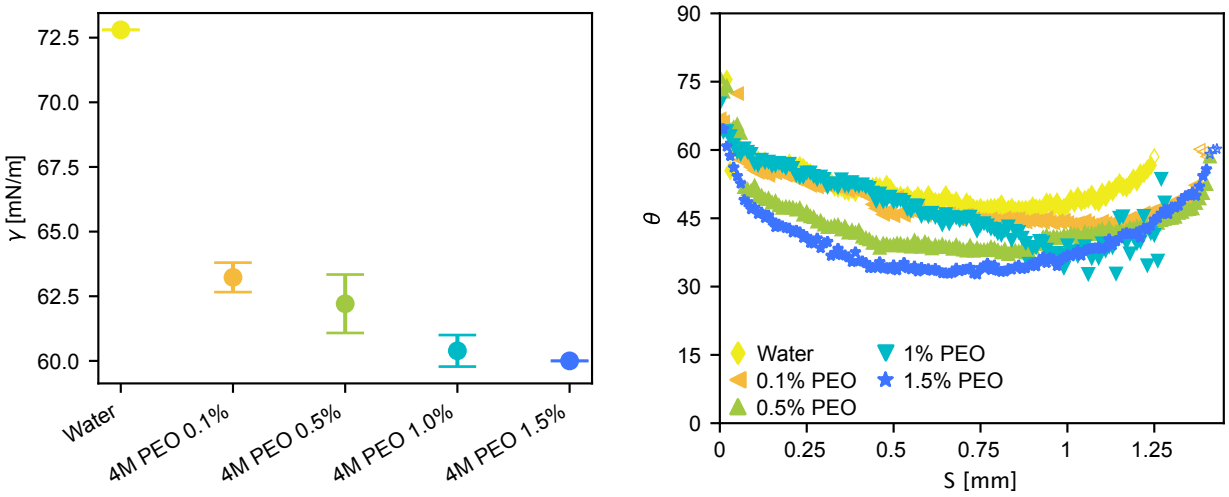

Figure S4: (a) Surface tension and (b) evolution of the contact angle (θ) as a function of the gap (S) between the particles for water and 4M PEO solutions of $c = 0.1 - 1.5$ %.

S5 Range of validity of the capillary-force approximation

The general expression for the capillary force at the neck of a liquid bridge is given by Willett *et al.* [6] as:

$$F = 2\pi\gamma R_{\min} - \pi {R_{\min}}^2 \Delta P \tag{S3}$$

where the Laplace pressure difference across the air-liquid interface is given by $\Delta P = \gamma(1/R_{\min} - 1/R_{\text{meridional}})$, with $R_{\text{meridional}}$ being the meridional (axial) radius of curvature. Using the analytical solution of the Young-Laplace equation for spheres under quasi-static conditions provided by Mielniczuk *et al.* [7], the pressure difference can be expressed as:

$$\Delta P = -2\gamma \frac{R_{\min} - R\sin\delta\sin(\delta+\theta)}{R^2\sin^2\delta - {R_{\min}}^2} \tag{S4}$$

where R is the bead radius, θ the solid-liquid contact angle, and δ is the half-filling angle. For our viscoelastic liquid-bridge study, the approximate expression $F \approx \pi\gamma R_{\min}$ (Eq. 3 in the main manuscript) corresponds to the case where the Laplace pressure term is $\pi {R_{\min}}^2 \Delta P \approx \pi\gamma R_{\min}$.

This condition $\pi {R_{\min}}^2 \Delta P \approx \pi\gamma R_{\min}$ requires the Laplace pressure to be $\Delta P \approx \gamma/R_{\min}$, which corresponds to a vanishing meridional (axial) curvature ($1/R_{\text{meridional}} \approx 0$), representing a cylindrical profile. Substituting $\Delta P \approx \gamma/R_{\min}$ into the Young-Laplace solution (Eq. S4) yields:

$$-2\gamma \frac{R_{\min} - R\sin\delta\sin(\delta+\theta)}{R^2\sin^2\delta - {R_{\min}}^2} \approx \frac{\gamma}{R_{\min}} \tag{S5}$$

which simplifies to:

$$\sin(\delta+\theta) \approx \frac{R^2\sin^2\delta + {R_{\min}}^2}{2R_{\min}R\sin\delta} \tag{S6}$$

Near contact ($S \to 0$), the neck radius is $R_{\min} \approx R\sin\delta$, simplifying this relation to:

$$\sin(\delta+\theta) \approx 1 \implies \delta+\theta \approx 90^\circ \implies \theta \approx 90^\circ - \delta \tag{S7}$$

For our experimental system (volume $V \approx 0.5-1$ μL on $R = 2$ mm beads), the half-filling angle is $\delta \approx 15^\circ$. Thus, the Laplace suction term is equal to $\pi\gamma R_{\min}$ when the contact angle is in the range of $\theta \approx 75^\circ$.

Our experimental measurements of the quasi-static contact angle (reported in Fig. S4(b)) show that at the start of separation ($S \to 0$), the contact angle lies precisely in the range $\theta \approx 60^\circ - 75^\circ$ across all concentrations due to contact line pinning. For this range of contact angles, $\sin(\delta+\theta)$ varies between $\sin(75^\circ) \approx 0.96$ and $\sin(90^\circ) = 1.0$, meaning that the approximation $\sin(\delta+\theta) \approx 1$ holds well. Consequently, the Laplace suction term is indeed well-approximated by $\pi {R_{\min}}^2 \Delta P \approx \pi\gamma R_{\min}$ in our system, and the force is well-described by the $F \simeq \pi\gamma R_{\min}$ approximation.

This behavior contrasts with the closest possible comparisons in the literature, namely the microgravity experiments by Mielniczuk *et al.* [7] and the mathematical modeling by Wang *et al.* [8]. While these studies provide valuable insights into capillary bridge shapes, their geometries and contact angles differ from ours. Specifically, Mielniczuk *et al.* utilized larger beads ($R = 4-5$ mm) and liquid volumes ($V = 1-10$ μL, corresponding to dimensionless volumes $V^* = V/R^3 \approx 0.016-0.15$), while Wang *et al.* modeled $R = 2.5$ mm spheres and fixed contact angle of $\theta \approx 0^\circ$ or 40°. Because their contact angles remain small compared to the zero-pressure condition ($\theta \approx 90^\circ - \delta \approx 75^\circ$ for our half-filling angle $\delta \approx 15^\circ$), their systems do not experience the pinning-induced suppression of the initial capillary force at small separations, resulting in $F \simeq 2\pi\gamma R\cos\theta$ rather than the $\pi\gamma R_{\min}$ model at early stages.

For our work, we were specifically interested in investigating viscoelastic liquid bridges at smaller, restricted volumes ($V \approx 0.5-1$ μL, corresponding to small dimensionless volumes $V^* = V/R^3 \approx 0.06-0.12$). This smaller volume regime is ultimately more representative of the pendular regime and relevant

to inter-particle cohesion in bulk wet granular systems, where liquid is confined to tiny capillary bridges at the contacts between grains [9]. In this pendular regime, the smaller bridge volume and large contact angle pinning minimize the relative importance of the Laplace pressure suction contribution, allowing the reduced $F \simeq \pi\gamma R_{\min}$ approximation to capture the force curves and the subsequent viscoelastic thinning dynamics remarkably well.

S6 Volume Measurement for the Liquid Bridge

The volume of the liquid bridge was calculated by treating the binarized 2-dimensional profile (see Fig. S5) as a solid of revolution. Assuming axisymmetry about the vertical axis, the total volume V is defined by the integral:

$$V = \int_{z_{min}}^{z_{max}} A(z)\, dz = \int_{z_{min}}^{z_{max}} \frac{\pi D(z)^2}{4}\, dz \tag{S8}$$

where $D(z)$ is the local diameter of the bridge at height z. To compute this from the image, the domain was discretized into N horizontal slices corresponding to the pixel rows. The volume was numerically approximated using a sum:

$$V \approx \sum_{i=1}^{N} \frac{\pi d_i^2}{4} \Delta z \tag{S9}$$

In this expression, d_i is the physical diameter of the bridge in row i, obtained from the pixel count n_i through $d_i = n_i/\alpha$, where α is the image calibration factor in pixels per mm. Likewise, $\Delta z = 1/\alpha$ is the physical height of a single pixel row. This summation yields the total volume in mm^3 (equivalent to μL).

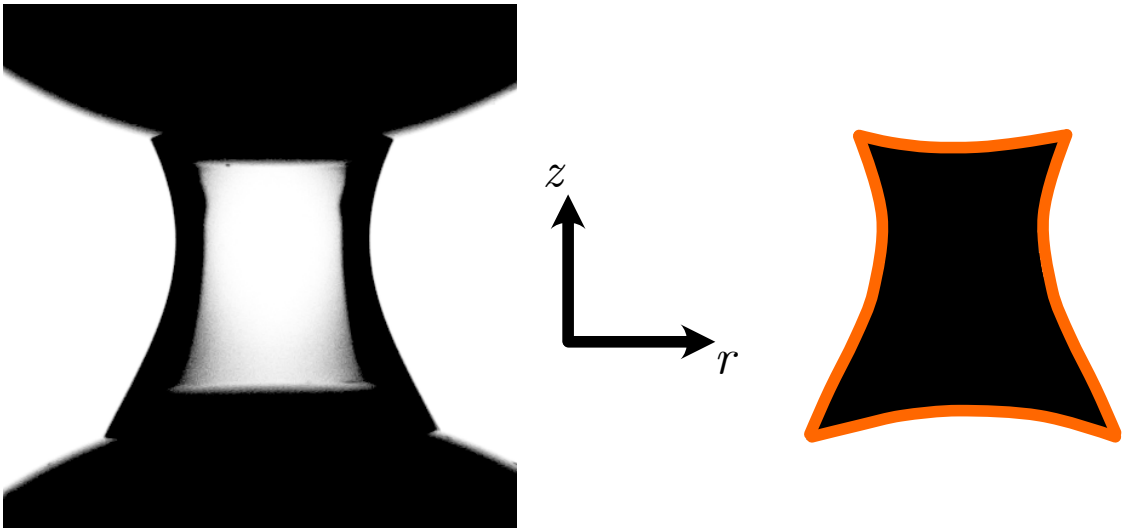

Figure S5: Contour used for measuring liquid bridge volume.

S7 Elastic Prefactor and Relaxation Time for $v = 0.01 - 10$ mm/s

In Fig. 5 in the main article, we fit the axial forces in the viscoelastic regime with the assumption that the force decays exponentially, where the resulting expression has the form:

$$F = F_c \exp\left(-\frac{S - S_c}{3v\lambda_e}\right) \tag{S10}$$

Here, S is the gap between the particles, S_c is the critical gap at the onset of the viscoelastic regime, and λ_e is the characteristic thinning timescale estimated from the recorded ligament dynamics. The only fitting parameter is F_c, the transition-force prefactor, which is summarized in Fig. S6(a) for 4M PEO at $c = 1\%$. We observe that F_c approaches a nearly constant value as v increases, while λ_e remains approximately independent of v.

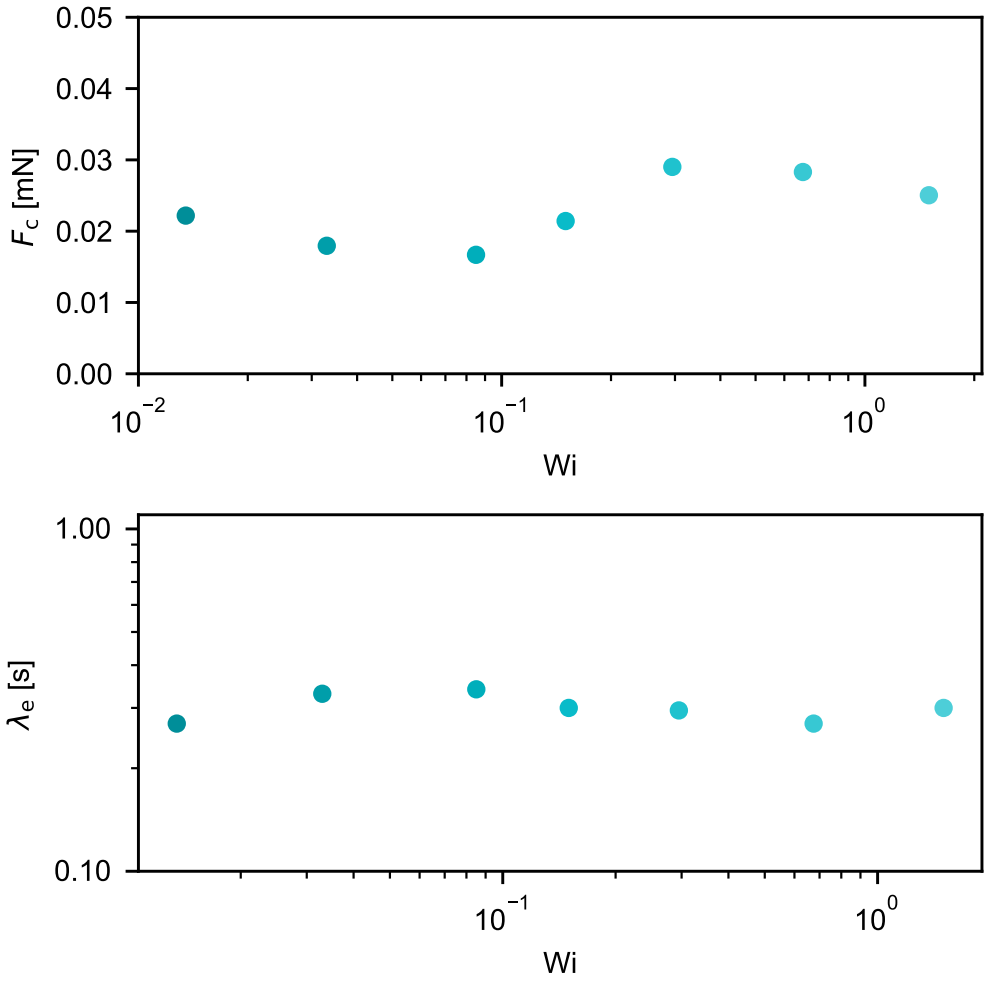

Figure S6: (a) Transition force F_c extracted from the exponential fit in the viscoelastic regime. (b) Characteristic timescale λ_e measured from the thinning dynamics of the liquid bridge for various separation velocities v.

S8 Particle-Particle Gap S_{peak} for Peak Axial Force

We define the gap, S between the particles where we measure the peak axial force during the particle separation (shown in Fig. 6 in the main article) as S_{peak}. In Fig. S7, we show S_{peak} for different concentrations of the polymer solutions for the range of velocities investigated in this work ($v = 0.01 - 10$ mm/s). The range considered for $S_{\text{peak}} \in [0.1 - 1]$ mm for the theoretical fits, shown in Fig. 6, is indeed reasonable based on experimental observations.

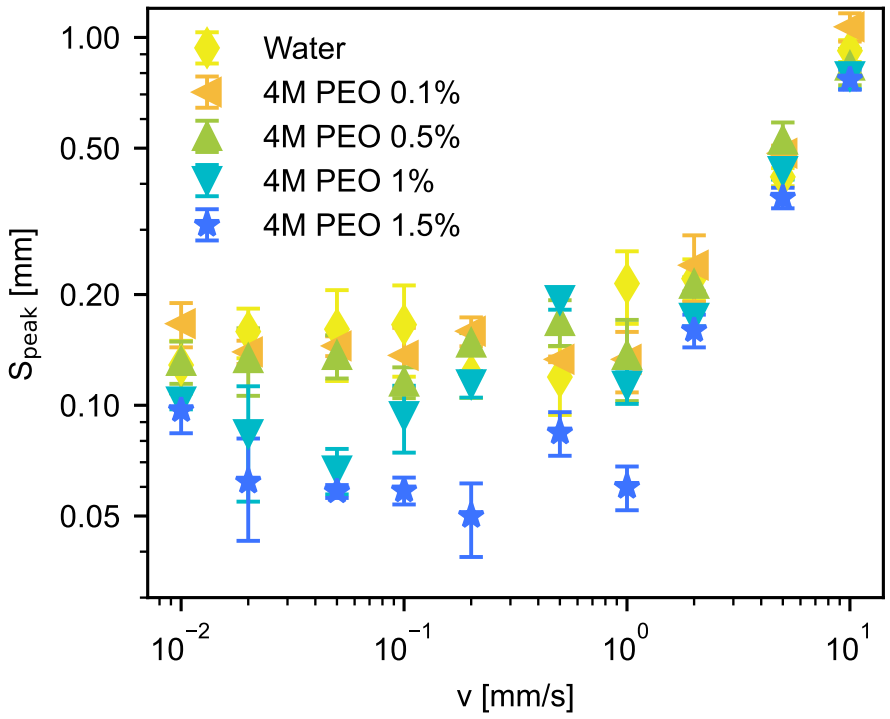

Figure S7: Gap corresponding to the peak force, S_{peak}, recorded for solutions of various concentrations at $v = 0.01 - 10$ mm/s.

S9 Role of Particle-size

Figure S8(a) shows the axial force as the particle separation increases at a velocity $v = 5$ mm/s for particle radii $R \in [1, 3]$ mm. The corresponding liquid bridge volumes are $V = 0.126, 0.42, 1, 2$, and 3.4 μL, respectively, chosen to approximately maintain the scaling $R \propto V^{1/3}$. The axial force exhibits initial Newtonian decay followed by a transition to the viscoelastic regime, with the final rupture distance depending heavily on V.

Figure S8(b) presents the evolution of the rescaled force, $F/\pi\gamma R$. The rescaled curves largely collapse across the different particle sizes. The slight deviation observed for $R = 1$ mm arises from experimental limitations in accurately loading such a small sample volume. Overall, these results illustrate that the standard scaling of capillary force with particle size remains valid for polymeric liquid bridges.

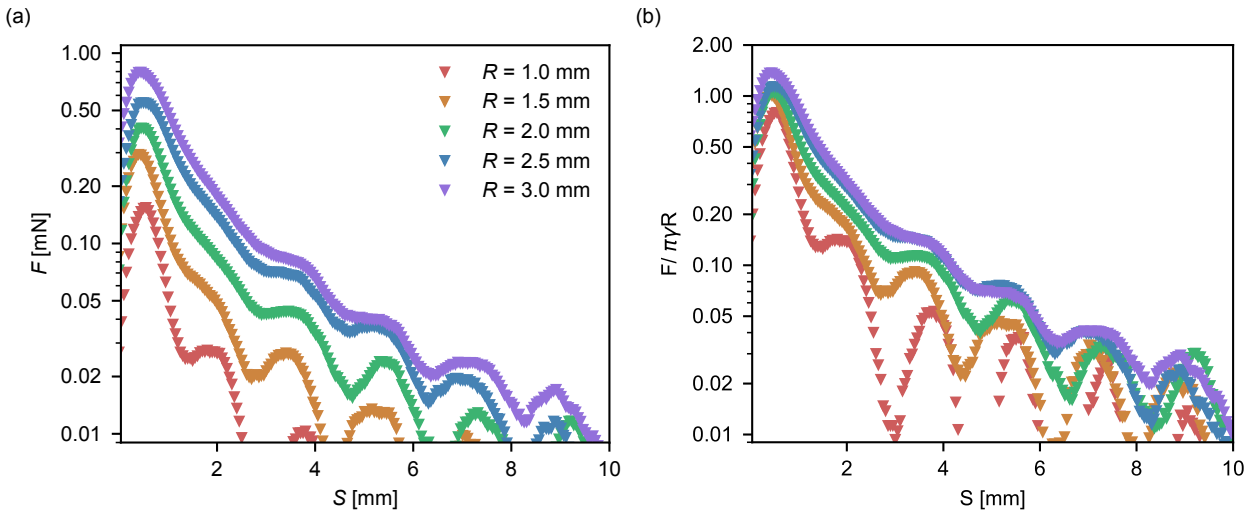

Figure S8: (a) Evolution of the axial force F with separation distance S for a 1 wt% 4M PEO solution at a fixed velocity $v = 5$ mm/s across varying particle radii R. (b) The rescaled evolution $F(S)/\pi\gamma R$.

References

[1] Olivier Pitois, Pascal Moucheront, and Xavier Chateau. Liquid bridge between two moving spheres: an experimental study of viscosity effects. *Journal of colloid and interface science*, 231(1):26–31, 2000.

[2] Guoping Lian, Colin Thornton, and Michael J Adams. A theoretical study of the liquid bridge forces between two rigid spherical bodies. *Journal of colloid and interface science*, 161(1):138–147, 1993.

[3] Sreeram Rajesh, Virgile Thiévenaz, and Alban Sauret. Transition to the viscoelastic regime in the thinning of polymer solutions. *Soft matter*, 18(16):3147–3156, 2022.

[4] Viyada Tirtaatmadja, Gareth H McKinley, and Justin J Cooper-White. Drop formation and breakup of low viscosity elastic fluids: Effects of molecular weight and concentration. *Physics of fluids*, 18(4), 2006.

[5] W. H. Cao and Mahn Won Kim. Molecular weight dependence of the surface tension of aqueous poly (ethylene oxide) solutions. *Faraday Discussions*, 98:245–252, 1994.

[6] Christopher D Willett, Michael J Adams, Simon A Johnson, and Jonathan PK Seville. Capillary bridges between two spherical bodies. *Langmuir*, 16(24):9396–9405, 2000.

[7] Boleslaw Mielniczuk, Olivier Millet, Gérard Gagneux, and Moulay Saïd El Youssoufi. Characterisation of pendular capillary bridges derived from experimental data using inverse problem method. *Granular Matter*, 20(1):14, 2018.

[8] Shaohan Wang, Fengyin Liu, Cheng Pu, Jingyu Cui, and Zhaolin Zeng. Mathematical study on gravity effect of the liquid bridge between two rigid spheres. *Powder Technology*, 407:117662, 2022.

[9] Vincent Richefeu, Moulay Said El Youssoufi, and Farhang Radjai. Shear strength properties of wet granular materials. *Physical Review E*, 73(5):051304, 2006.